INL/CON-18-44479-Revision-0

Microstructure and Fission Product Distribution Examination in the UCO kernel of TRISO Fuel Particles

I. J. van Rooyen, Y. Yang, T. Holesinger, Mukesh Bachhav, Z. Fu

October 2018

The INL is a U.S. Department of Energy National Laboratory
operated by Battelle Energy Alliance

INL/CON-18-44479-Revision-0

Microstructure and Fission Product Distribution Examination in the UCO kernel of TRISO Fuel Particles

I. J. van Rooyen, Y. Yang, T. Holesinger, Mukesh Bachhav, Z. Fu

October 2018

Idaho National Laboratory
Idaho Falls, Idaho 83415

http://www.inl.gov

Prepared for the
U.S. Department of Energy

Under DOE Idaho Operations Office
Contract DE-AC07-05ID14517

Proceedings of HTR 2018
Warsaw, Poland, October 8-10, 2018
Paper HTR 2018-3012

Microstructure and Fission Product Distribution Examination in the UCO Kernel of TRISO Fuel Particles

I.J. van Rooyen, Z. Fu[1], Y. Yang[1], T.G. Holesinger[2], and M. Bachhav[3]
Fuel Design and Development Department, Idaho National Laboratory
PO Box 1625, Idaho Falls, Idaho 83415, U.S.A.
phone: +1-208-5264199, Isabella.vanrooyen@inl.gov

[1]*Materials Science and Engineering Department, University of Florida, Gainesville, FL, U.S.A.*

[2]*Nuclear Materials Science, Los Alamos National Laboratory, Los Alamos, NM, U.S.A.*

[3]*Advanced Characterization Department, Idaho National Laboratory, Idaho Falls, ID, U.S.A.*

Abstract – *The effect of the irradiation and fabrication processes on the UCO fuel kernel, kernel-buffer interlayer, and fission products has not been fully studied for UCO fuel kernels of tristructural isotropic (TRISO) coated particles. Specifically, the fission product retention, composition, and distribution within these structures for TRISO fuel performance at normal and accident conditions are not well reported in literature. Structural and chemical information in the irradiated UCO fuel kernel (e.g., the stoichiometry variations) may further contribute to fuel performance modeling under the Nuclear Energy Advanced Modeling and Simulation Program. The microstructural and micro-chemical evolution of selected irradiated UCO fuel kernels, kernel-buffer interfaces, and recoil zones were characterized using scanning transmission electron microscopy and energy dispersive spectroscopy elemental mapping. An atom probe tomography technique is employed to determine three-dimensional microstructure and chemical mapping at nanometric length scale of a safety-tested fuel particle UCO kernel. Fuel kernels from an unirradiated coated particle and irradiated Advanced Gas Reactor kernels from the first and second experiments irradiated to 17.4% fissions per initial metal atom (FIMA) and 12.55% FIMA, respectively, were examined. The following main findings were made from the irradiated kernels examined: (1) resultant microstructure after irradiation consists of two primary phases, a "high-Z (atomic mass)" UC(O) phase (rock salt; a=0.496 nm) and a "low-Z" UO_2(C) phase (fluorite structure; a = 0.547 nm); (2) UC phase containing Zr, Mo, and/or Ru with Zr and Mo show segregation into distinct grains; (3) Xe bubbles were found almost exclusively in the high-Z phase (UC(O)) and in the examined AGR-1 particle, the Zr-containing phase within the UC(O) fuel phase; and (4) APT data reveals segregation of Te and Ag at the UO-UC interface.*

I. INTRODUCTION

A variety of irradiation experiments were completed at Idaho National Laboratory (INL) on tristructural isotropic (TRISO) coated particles contained in a graphitic matrix. Fuel tested in the AGR-1 and AGR-2 experiments has kernels composed of a mixture of UO_2 and UC with a nominal as-fabricated stoichiometry of $UO_{1.37}$ $C_{0.35}$ and $UO_{1.43}$ $C_{0.39,}$ respectively [1-3]. These as-fabricated kernel stoichiometry values are determined at the completion of kernel fabrication and do not account for, any changes that will occur during the subsequent coating and compacting processes.

Earlier fuel kernel examinations provided knowledge on fission product distributions in different fuel types (UO_2, UC_2, PuO, and ThO_2-PuO) irradiated at different conditions that are relevant to

the AGR-1 and AGR-2 experiments. Fission product distribution has been studied in various types of layered nuclear fuel particles for several decades [4-8]. Although Tiegs studied fission product distribution in UCO kernels with particular attention to corrosion of the SiC layer by Pd, the UCO particles had a C:O ratio of about 4:1, while those in the AGR-1 experiment have a C:O ratio of about 1:4.3.

Work to date studying fission product distribution in AGR-1 UCO safety-tested kernels using electron probe micro-analyses showed that volatile fission products such as Cs, I, and Xe are not fully retained in the kernel, but rather they accumulate significantly in the buffer layer [9]. Barrachin et al. [5] suggests that a large portion of Xe remains in atomic form in the fuel matrix and moves by diffusion toward grain boundaries. Once it reaches the grain boundaries, it can travel via interconnected pores formed by high temperatures. The mechanism for Cs movement is similar, except that they postulate that Cs can travel as an oxide or iodide.

We therefore aim to understand the distribution and chemical composition of fission products in the kernel, and to gain knowledge of the effect that the irradiation level has on the UCO micro- and nanostructures.

II. EXPERIMENT, SAMPLE DESCRIPTION, AND METHODS

These initial studies focused on the changes in fuel phases, chemical composition, and distribution of fission products due to neutron irradiation. This paper describes the unirradiated microstructure from a coated particle (not compacted) from the AGR-1 experiment, and one irradiated kernel's microstructure from both the AGR-1 and AGR-2 experiments, using scanning transmission electron microscopy (STEM) and energy dispersive spectroscopy (EDS) examination. (See Table 1 for the irradiation history of selected samples.)

Microstructure, chemical composition, and selected area diffraction (SAD) characterizations were conducted using three transmission electron microscopes (TEMs) at different locations. The FEI Tecnai G2 F30 STEM at the Center for Advanced Energy Studies (CAES) at INL operates at 300 kV with the STEM HAADF resolution of 1.9 Å. The TEM at the University of Florida is a FEI Tecnai F20 S/TEM operating at 200 kV with a 1.6 Å resolution in high-angle annular dark field (HAADF) imaging, and it is equipped with a EDAX r-TEM super ultra-thin window Si(Li) EDS detector.

The microscope used at Los Alamos National Laboratory (LANL) is an image-corrected FEI Titan operated at 300 kV, with a point-to-point resolution of 0.7 Å in image (TEM) mode. High-resolution STEM imaging resolution is 1.4 Å. Spectral images were collected in STEM mode, and the STEM spectral image data were collected at 300 keV with an estimated analytical probe size of 1.4 nm. These data were captured with an EDAX Si-windowed spectrometer with a 0.13 steradian collection angle. Each of the elements was quantified based on a standardless k-factor quantification using 300 keV and a modelled sample thickness correction using FEI's commercial TEM imaging and analysis software. Based on a 3:1 threshold intensity criterion over background, peak intensities were subsequently integrated, quantified, and reported. Fission product elements with measured concentrations above the detection limits were taken to be present, and those with measured concentrations below the detection limits were taken to be absent.

Table 1: Neutron irradiation parameters of AGR-1 and AGR-2 experiments (*safety tested 1600°C).

Compact	AGR1-523-SP01	AGR2-223-RS006	AGR1-433-004*
Burnup (% fissions per initial metal atom [FIMA])	17.4	12.68	18.6
Fast neutron fluence (x 1025 n/m^2) E>0.18 MeV	3.77	3.46	4.16
Time-average volume-average temperature (°C)	1059	1296	1094
Time-average peak temperature (°C)	1141	1360	1179
Ag retention (% measured to calculated ^{110m}Ag [10])	16	8	98
U-enrichment (atom %) [2, 3]	19.74	14.03	19.74

Additionally, atom probe tomography (APT) examination was performed on a safety-tested fuel sample (AGR1-433-004), as part of a National Users Facility Rapid Turnaround Project. The APT technique is employed to determine three-dimensional (3-D) microstructure and chemical mapping at nanometric length scale. The objective was to obtain atomic chemical composition for quantification of the fuel phases as well as quantification of fission product phase distributions.

In APT, atom-by-atom removal from the surface of a needle-shaped specimen (radius usually ~100 nm) is accomplished by a field-assisted evaporation process. The needle is usually cooled down to cryogenic temperatures of 20–80 K and subjected to a very high electric field (few 10s V/nm) in addition to laser pulses to enable the field evaporation process. APT specimens were prepared by standard lift-out and milling procedures using a FEI Helios plasma focused ion beam (FIB) instrument. Data acquisition

was performed using a Cameca LEAP 4000X HR instrument operated in laser mode with energy of 150 pJ/pulse, a pulse repetition rate of 200 kHz, and data collection rate of 5 atoms per 1000 pulses. The specimens in LEAP were cooled to a base temperature of 50 K. Data analysis was completed with the CAMECA Integrated Visualization & Analysis Software (IVAS), Version 3.6.8. The datasets were reconstructed using a radius determined from a scanning electron microscope image. The reconstruction parameters ranged between an image compression factor between 1.4 and 1.5 and k-value between 3.1 and 3.5.

III. RESULTS

Microstructural examinations were completed on an AGR-1 experiment unirradiated UCO fuel kernel (as-fabricated and coated), one AGR-1 fuel kernel irradiated to 17.4% FIMA and one AGR-2 fuel kernel irradiated to 12.68% FIMA, respectively.

III.A. Microstructure of an Unirradiated UCO AGR-1 Kernel

The most significant structural changes comparing the as-fabricated and irradiated fuel materials (Fig. 1) are the presence of porosity, much smaller grain sizes, and the absence of material structurally similar to UC_2 in the irradiated material. The unirradiated fuel consists of UO_2, UC_2, and UC regions (Fig. 1(a)). The UC_2 (containing O) was found to be tetragonal with a = 0.495 nm and b = 0.595 nm. Identification of the UC phase is shown in Fig. 2 where the area indicated in the TEM bright field images (a) and (b) was used for the diffraction patterns (c) and (d). The UC phase (containing some O) was found to have a cubic structure with a = 0.495 nm. The only orientation relationship the UC phase found was parallel alignment to the cube faces of the UC_2 phase with $[010]UC_2 \parallel [010]UC$ and $(001)UC_2 \parallel (001)UC$.

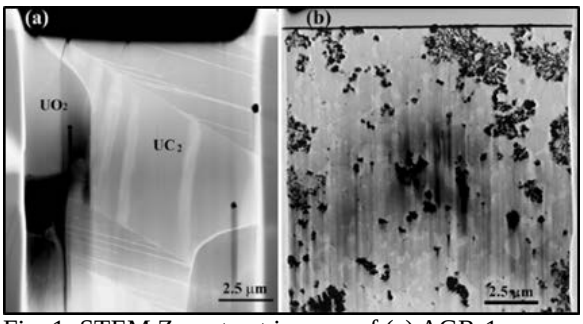

Fig. 1: STEM Z-contrast images of (a) AGR-1 unirradiated fuel from Particle AGR1-T6051-1 and (b) irradiated fuel from Particle AGR1-523-SP01, showing the considerable changes in structure the fuels undergo during neutron irradiation.

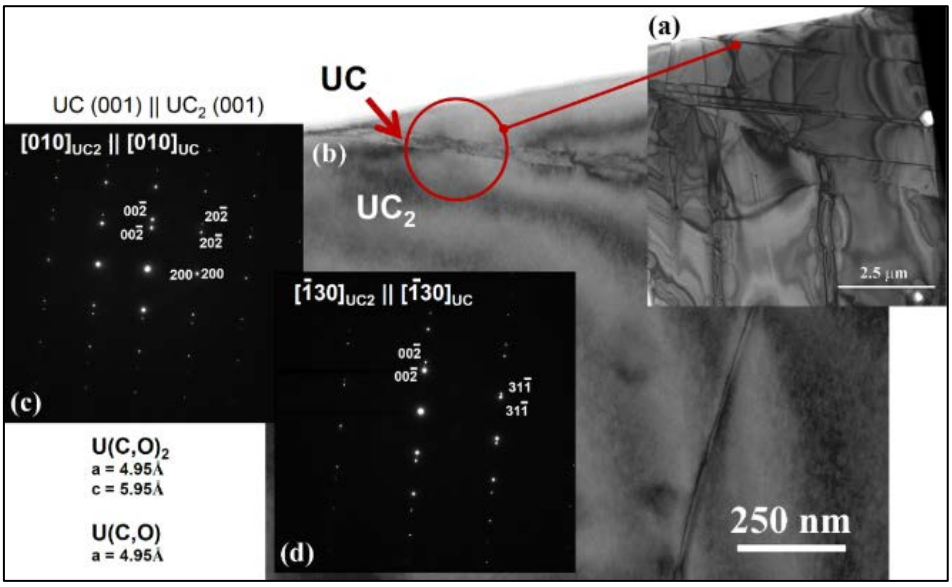

Fig. 2: Identification of the UC phase and orientation relationship to UC_2 from TEM images from unirradiated Particle AGR1-T6051-1 (a) and (b) with SAD patterns (c) and (d) taken from the area indicated.

Higher-magnification images of the structure of the fuel taken from the edge of the fuel kernel are shown in the TEM images (Fig. 3). These suggest some strain build-up, presumably due to a lattice mismatch between the UC_2 and UC phases. This is readily apparent in Fig. 3(a) when viewing the strain contrast along the interfaces between the UC platelet and the UC_2 host material. This is less obvious in Fig. 3(b) where at least some of the observed contrast comes from specimen bending and thickness variations.

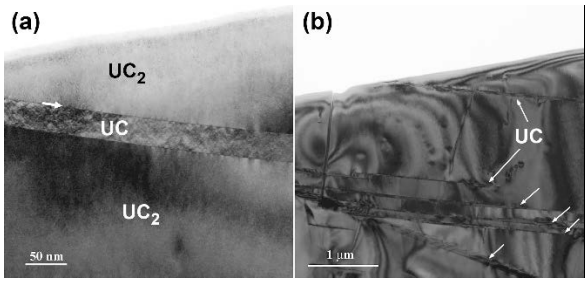

Fig. 3: Images of the structural arrangement (Widmanstatten) of the UC platelets within the UC_2 host phase from unirradiated Particle AGR1-T6051-1. The TEM bright field images (a) and (b) suggest residual strain exists along the boundaries arising from this arrangement.

III.B. Microstructure of Irradiated UCO Kernels from the AGR-1 Experiment

The irradiated fuel from Particle AGR1-523-SP01 consisted of two primary phases, namely the "high-Z" mono-carbide phase (UC) and the "low-Z" U oxy-carbide phase, where UO_2 (fluorite, a = 0.547 nm) also contains some carbon (Fig. 4). The UC is referred to as the high-Z phase due to its higher average atomic number. However, EDS analysis showed that the UC phase contained O along with Zr, Mo, and /or Ru.

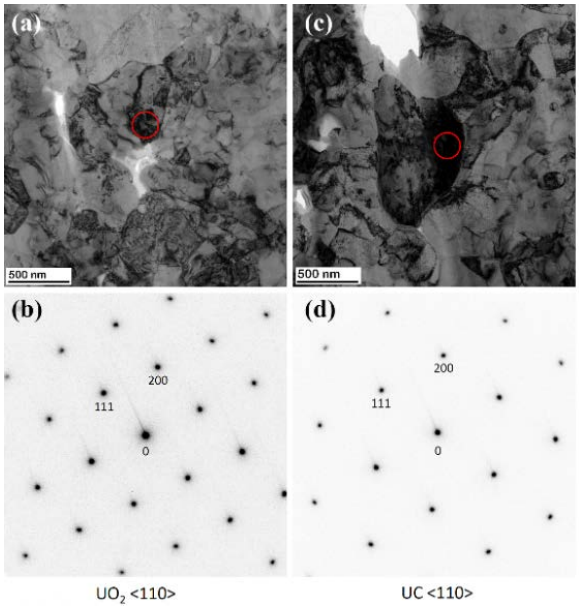

Fig. 4: Bright field and SAD pattern pairs from random grains from the AGR1-523-SP01 fuel kernel containing (a, b) UO_2, and (c, d) UC structures.

The UO_2 phase was found by EDS to contain some carbon, along with trace amounts of I, Cs, Pr, Er, and Nd. UC is present as both inclusions within the UO_2 type material and as small grains decorating the grain boundaries of the UO_2 phase. The UC phase did not contain precipitates of the low-Z oxy-carbide material. The elements Zr, Mo, and Ru were often observed as segregated into separate UC grains.

The overall chemistry of the fuel center is shown in Fig. 5. The high-Z material (bright phase) is the UC phase containing Zr, Mo, and/or Ru. Note that the spectral images for Zr and Mo show the segregation of these elements into distinct grains. The low-Z, UO_2 material contains low levels of Cs, Ce, and Nd as shown in the spectral images. This was confirmed by several long EDS spot spectra, which clearly showed these peaks. The presence of graphite in the small particulate mixture in the large pores of the matrix is indicated by the carbon spectral image.

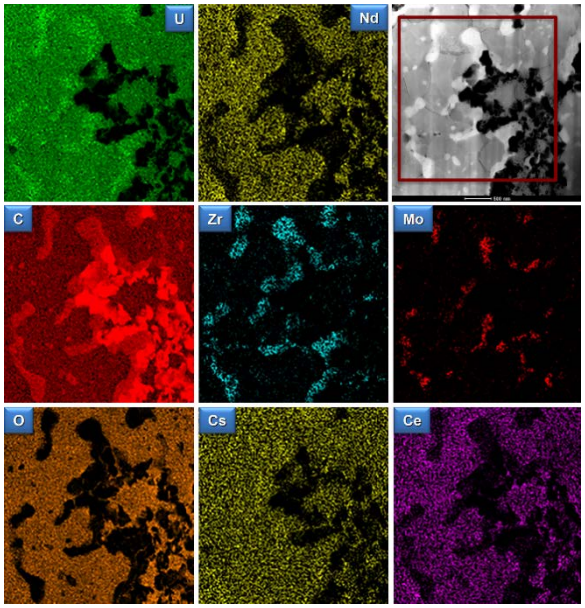

Fig. 5: STEM EDS spectral images taken from the indicated scan area in the Z-contrast image of the AGR1-523-SP01 fuel kernel central region.

Fig. 6 contains a higher-magnification STEM image and elemental spectral images from the fuel kernel center specimen. Again, the Mo and Zr in the high-Z material are clearly segregated into distinct grains. There are a number of pores in the high-Z material that contain Xe (see specifically the white arrows in Fig. 6). Very few pores were found within the low-Z material. The smaller precipitates of the high-Z material within the low-Z grains also displayed the chemical segregation between the Zr, Mo, and Ru.

Confirmation of Xe within these bubbles is obtained with longer dwell-time spot spectra. Shown in Fig. 7 is a STEM Z-contrast image with bubbles residing in the Zr-containing UC phase. In general, it was found that the majority of the Xe bubbles are in the Zr-containing UC phase. Not all bubbles that are suggested by the Z-contrast images contain Xe. Some of the bubbles may have been breached in the FIB preparation process, letting the Xe escape. Some of the intensity in the Xe map is just noise from the mapping process due to the short acquisition times and low count rates with the current detector system. However, small bubbles of Xe not readily visible in the STEM image cannot be ruled out. This potential preference for Xe residence in one of the phases is an aspect that will continue to be examined in follow-on work.

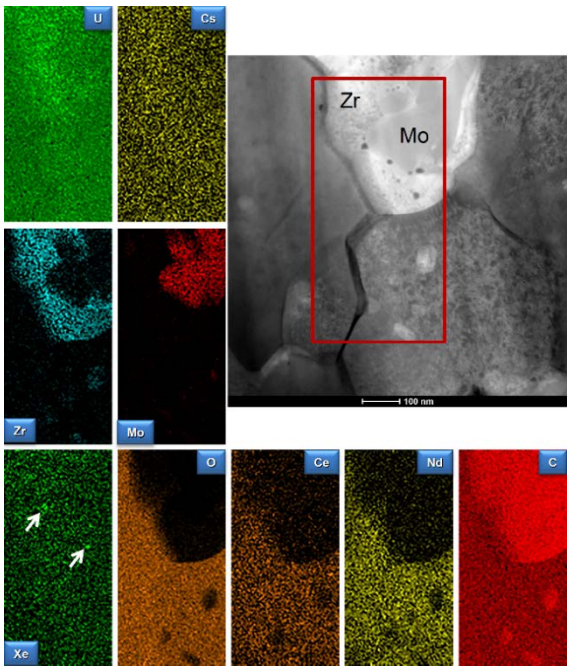

Fig. 6: STEM Z-contrast image and corresponding spectral images for U, Zr, Mo, Xe (arrows indicate Xe bubbles), Ce, Nd, C, and O from the indicated scan area of the fuel kernel of Particle AGR1-523-SP01.

III.C. Microstructure of Irradiated UCO Kernels from the AGR-2 Experiment

AGR-2 kernels are inherently different from those of AGR-1 experiments, specifically with regards to the U-enrichment level (14.03% versus 19.74%), kernel diameter (426.671 µm versus 349.506 µm), and stoichiometry [2, 3].

Three TEM lamellae were prepared from the mounted fuel Particle AGR2-223-RS06 at positions of the fuel center (#1), the edge of the fuel kernel (#2), and at the interface between the fuel kernel and carbon buffer layer (#3), respectively. Due to the relatively large thickness of lamellae #2 and #3, aggravated by heavy elements in the specimen, SAD patterns were only conducted on lamella #1.

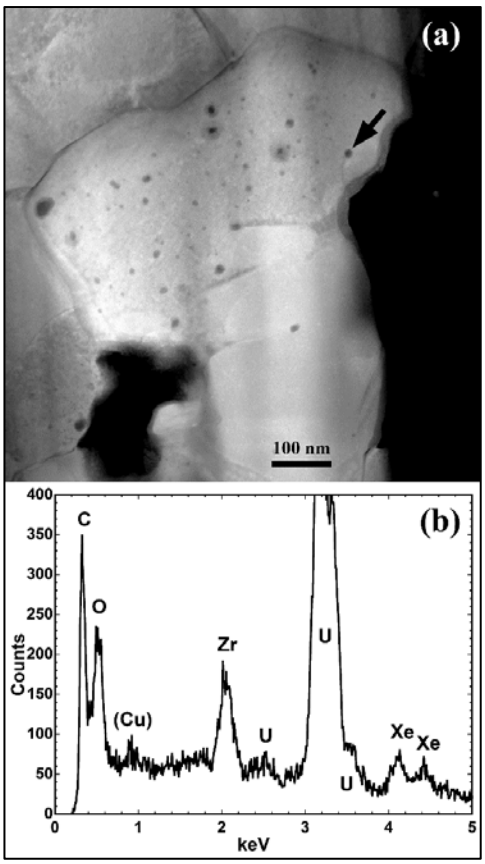

Fig. 7: Z-contrast (a) STEM image of bubble formation in the Zr-containing UC phase. The spectra with the Xe peaks in (b) is from the indicated bubble in (a). The Cu peak is an artifact from fluorescence of the Cu grid that holds the FIB specimen.

Fig. 8 shows the low-mag overview Z-contrast image of lamella #1. Clearly, as compared with the microstructure of the unirradiated fuel kernel, there are significant reconstructions and phase evolutions occurring in the irradiated fuel kernel [11]. The microstructure is featured with irregularly shaped pores, phases with a higher average Z showing in bright contrast, and phases with a relative lower Z in gray to dark contrasts. Totally, six AOIs were examined, including three using conventional TEM imaging, spot EDS, and SAD, and the other three using STEM/EDS mapping.

Fig. 9 shows the TEM images from AOI #1 to AOI #3. Scattered voids or gas bubbles are clearly apparent, particularly along the phase interfaces and in the phases with a bright contrast in the HAADF image. The large precipitate in AOI #2 shows as amorphous base on the diffraction pattern, while P1 in AOI #3 has a bcc crystal structure determined from two diffraction patterns at different zone axis.

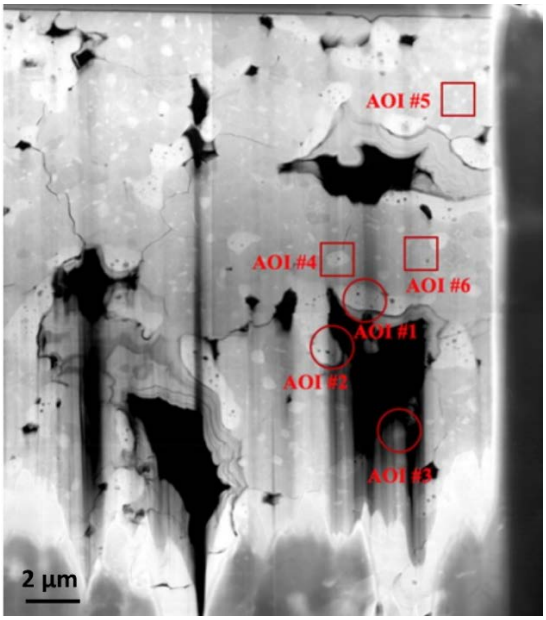

Fig. 8: Overview Z-contrast STEM HAADF image of lamella #1 from Particle AGR2-223-RS06 with areas of interest (AOIs) labeled (square: STEM elemental map; circles: conventional TEM, Spot EDS, and/or SAD).

The chemical compositions from evaluated positions and particles are listed in Table 2. Due the high uncertainties in C and O measurements, the purpose of listing compositions is only to show relative concentrations of heavy elements. Zr is present at all positions except AOI #1 P2. The AOI #1 P2 is enriched with Nb and Mo, which is consistent with our EDS mapping results showing that Mo and Nb tend to precipitate out from large Zr-enriched phases. The amorphous particle AOI #2 P1 is enriched with Ru and Rh.

Fig. 10 shows the STEM EDS map of an isolated phase in bright contrast, which is enriched with Mo, Nb, and Zr. Interestingly, the large black dot located at the center of this isolated particle shows Kr, C, O, Nd, and Pr, and it is highly suspected that this Kr gas bubble is encapsulated in a shell of C, O, Nd, and Pr. However, more EDS maps at higher spatial and spectral resolutions on the similar features are needed for proving our speculation. Cs and Xe co-precipitates are also spotted at the phase boundary.

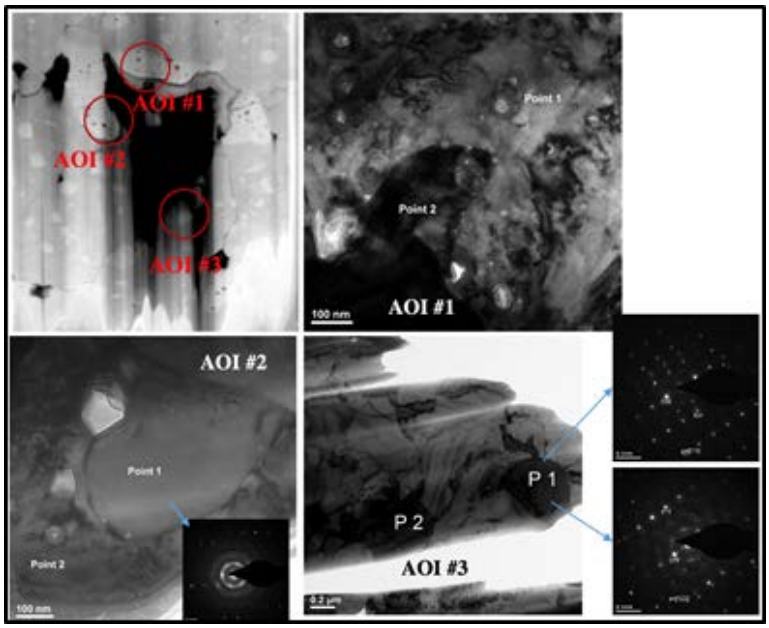

Fig. 9: TEM images of three AOIs (AOI #1 to AOI #3 in Fig. 8) and SADs from Particle AGR2-223-RS06.

Fig. 11 is the EDS map from AOI #5 of lamella #1, and these three mid-size bright precipitates are all enriched with Zr. More detail examinations show that precipitate 1 (as labeled on the Zr map) actually consists of two parts. The upper part is enriched with Zr, and the lower part is enriched with Tc, Ru, Mo, Nb, and C. Precipitate 3 also consists of left and right parts with different element enrichments.

Fig. 12 is the EDS map of AOI #6 (shown in Fig. 8), which includes a relatively large bright phase and multiple fine precipitates. Consistently, those bright phases are generally enriched with Zr but depleted of O and U. Within the large Zr-rich bright phases or at their close proximity, nucleation of Mo, Nb, Tc, and Ru enriched precipitates are observed. The precipitate highlighted in a dash line circle clearly shows as a (Zr, Nb, Mo) carbide. Cs precipitates were only observed in lamella #1 AOI #4 (Fig. 10), where the large Zr-rich precipitate were examined. Cs and Xe co-precipitates into very fine particles. Overall, Cs is depleted from the Zr-rich areas.

Table 2. Chemical composition (wt%) from interested position and particles highlighted in Fig. 9.

Position/Particle	C	O	U	Zr	Ru	Nb	Mo	Rh
AOI #1 P1	33.0	8.9	51.0	7.1				
AOI #1 P2	36.3	2.6	45.7			0.2	15.2	
AOI #2 P1	26.9	4.0	34.9	0.6	17.6			16.1
AOI #2 P2	27.6	24.4	41.8	6.2				
AOI #3 P1	44.8	9.3	42.2	3.7				
AOI #3 P2	32.9	6.6	46.6	13.8				

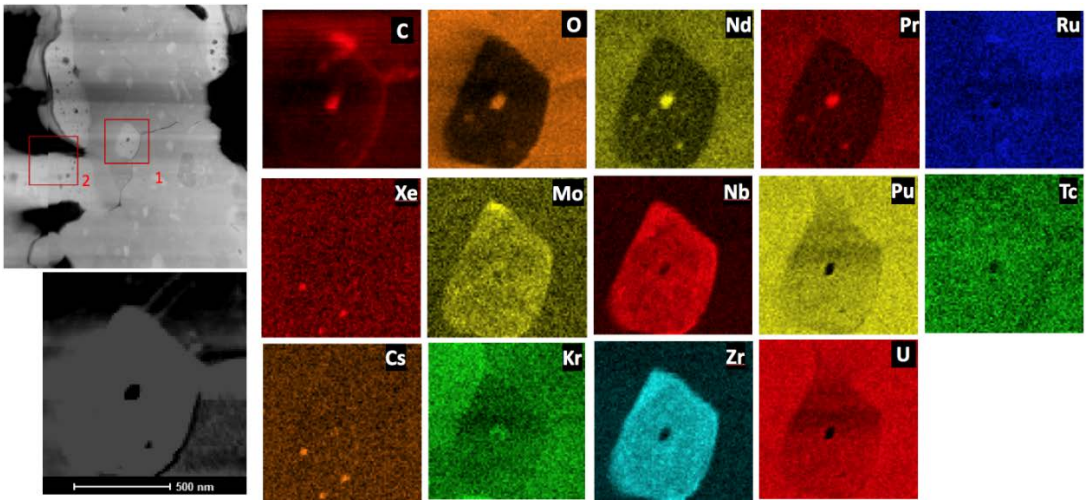

Fig. 10: STEM EDS map of an isolated phase from AOI #4 (shown in Fig. 8) from Particle AGR2-223-RS06.

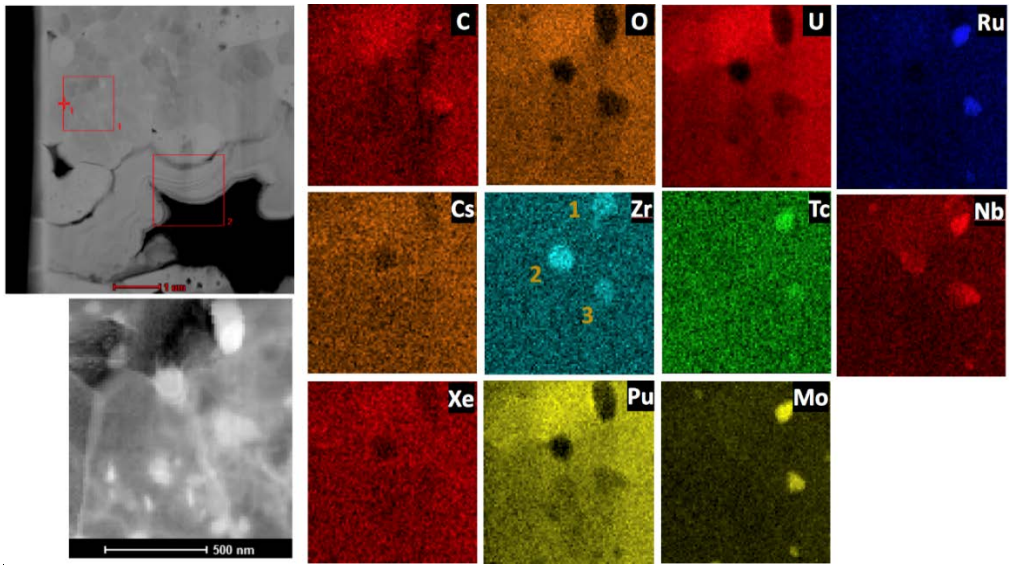

Fig. 11: STEM EDS map of multi-fine precipitates (AOI #5 shown in Fig. 8) from Particle AGR2-223-RS06.

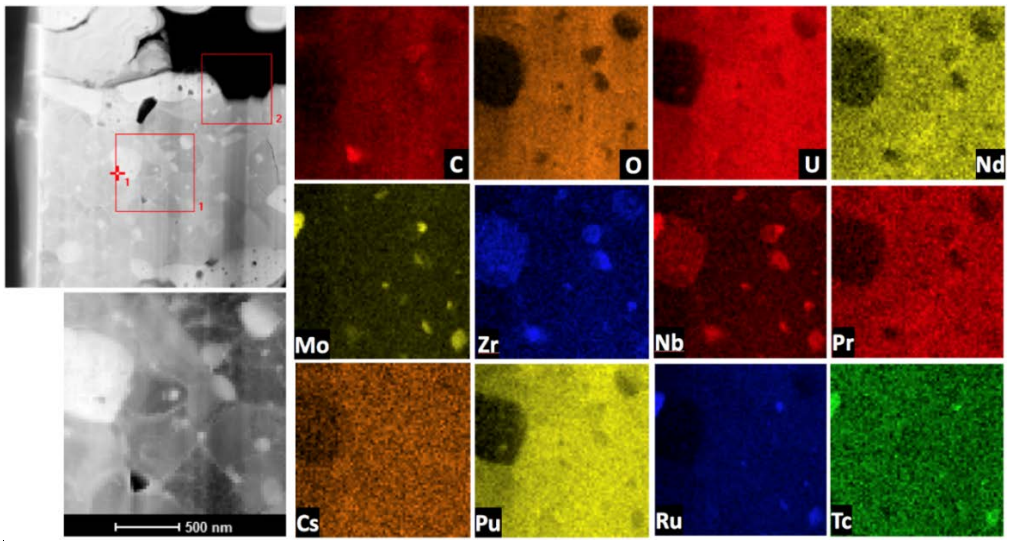

Fig. 12: STEM EDS map of area from Particle AGR2-223-RS06 including large bright phase and fine precipitates taken from AOI #6 (shown in Fig. 8).

As stated previously, only TEM/STEM imaging was conducted due to the thickness of lamella #2, and it was mainly aimed to confirm the nature of the scattered dark phases. The irregularly shaped dark phase in Fig. 13(a) is actually carbon or graphite instead of being just a pore (shown as bright contrast areas in Fig. 13(b)). As indicated by the white arrows, those two areas actually show fibrous structure, which definitely cannot originate from mount resin. It can also be seen that the concentration level of the dark contrast phase decreases as from the outer fuel region to the center of the fuel, but there is no obvious change in the lamella vertical direction, which indicates that those carbon/graphite inclusions originated from the carbon buffer layer fabrication or diffusion of carbon buffer layer into the fuel under irradiation. Some isolated U-containing particles were located in the buffer layer.

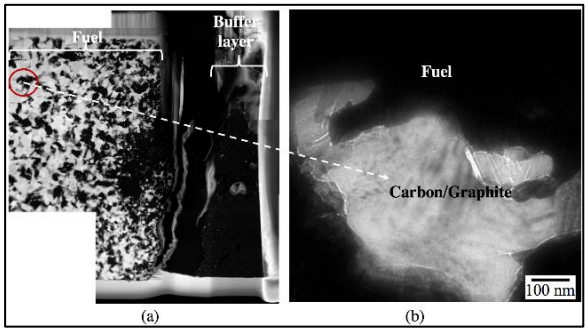

Fig. 13: (a) HAADF STEM image of lamella #2; (b) conventional TEM image of circulated area in (a).

For lamella #3 (Fig. 14), those dark phases in the STEM image (Fig. 14(a)) are identified as carbon/graphite by spot EDS analysis. The electron transparency also shows that these phases consisting of light elements (Fig. 14(b-d)). Spot EDS from points 1 and 2 in AOI #3 (lamella #3, edge of kernel) also shows that Nb tends to precipitate out from the neighboring large Zr-rich phase (Table 3).

Fig. 15 shows the EDS map of AOI #4 in lamella #3. Clearly, these fine precipitates are enriched with Zr, Mo, Nb, and C, and some of them also have a high concentration of Ru, Rh, and Tc. It is worth noting that the large Zr-rich phase at the bottom-right corner contains nearly no Mo, Tc, Rh, or Ru, but it does contain Nb, which is consistent with the observation in the EDS maps from lamella #1 that Mo, Rh, Tc, and Ru might co-precipitate into an epsilon phase [12].

Table 3. Chemical composition (wt%) from the positions highlighted in AOI #3 of Fig. 14.

Element	C	O	U	Zr	Nb
AOI #3 P1	24.18	11.88	60.78		3.14
AOI #3 P2	26.6	3.03	55.04	13.0	2.3

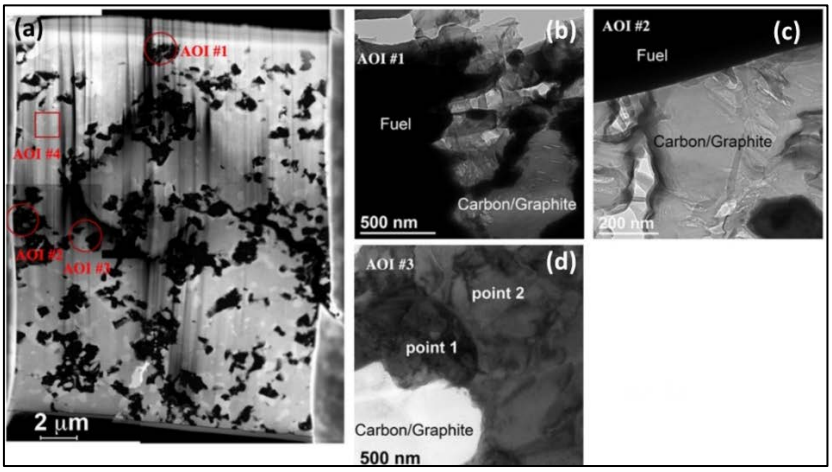

Fig. 14: (a) HAADF STEM image of lamella #3 from Particle AGR2-223-RS06 and (b-d) conventional TEM images from AOIs.

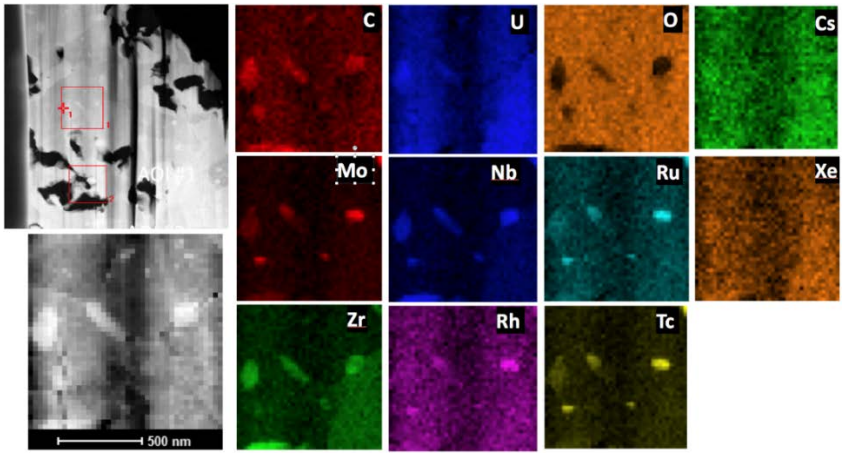

Fig. 15: EDS map taken from AOI #4 (see Fig. 14) in lamella #3 from Particle AGR2-223-RS06.

III.D. Atom Probe Tomography of a Safety-Tested AGR-1 Fuel Particle

Chemical analysis from fission products from a UCO kernel from a safety-tested (1600°C, 300 h [13]) AGR-1 particle (AGR1-433-004) were performed using APT. The APT specimen was prepared from the center of the fuel particle and the corresponding 3-D dataset is shown in Fig. 16(a) across the interface of the UO and UC phase with corresponding iso-concentration surface. The analyzed cylinder (radius 15 nm, 40 nm length) is shown in Fig. 16(a) with dotted lines. The distribution of selected fission products across the interface of the UO and UC phase is shown in Fig. 16(b). APT data reveals segregation of Te and Ag at the UO and UC interface. The UO phase showed presence of fission products such as Pd, Zr, Ce, Nd, Er, Dy, Gd, La, Y, Xe, and Sm, whereas the UC phase showed higher concentrations or segregation of Rh, Ru, Zr, Xe, Cd, In, Sn, Tc, and Nb. No Cs was detected during this investigation (only selected fission product distribution are shown in Fig. 16(b)).

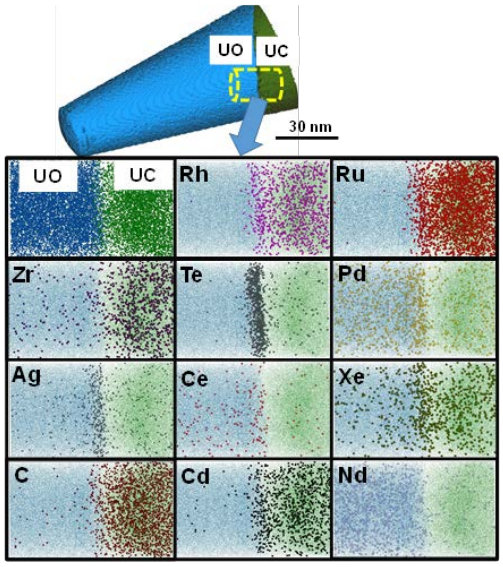

Fig. 16: 3-D APT data obtained the center of UCO kernel fuel particle. (a) 3-D reconstructed tip with iso-concentration surfaces highlighting UO and UC phase. (b) 3-D interfacial distribution of fission products Rh, Ru, Zr, Te, Pd, Ag, Ce, Xe, Cd, and Nd across the UO and UC phase.

IV. CONCLUSIONS

Fuel kernels from AGR-1 and AGR-2 compacts irradiated to 17.4% and 12.5% FIMA, respectively, were examined and compared with an unirradiated AGR-1 UCO fuel kernel (as-fabricated and coated). The following main findings were made:

- The microstructure of the unirradiated fuel kernel exists of UO_2 and UC_2 with UC platelets.
- The resultant microstructure after irradiation consists of two primary phases, namely a "high-Z (atomic mass)" UC(O) phase (rock salt; a=0.496 nm) and a "low-Z" UO_2(C) phase (fluorite structure; a = 0.547 nm).
- The UO_2 phase contained multiple precipitates of the UC phase, whereas no precipitates of the UO_2 phase were identified in the UC phase.
- The UC phase contained Zr, Mo, and/or Ru, and the UO_2 phase contained trace amounts of I, Nd, Pr, Cs, Ce, and Er.
- The STEM-EDS analysis of the AGR-1 particle shows Xe bubbles almost exclusively in the Zr-containing part of the UC phase. APT analysis on a safety tested AGR-1 particle also shows Xe preference for the UC phase, although Xe were also identified in the UO_2 phase.
- Interaction between the fuel kernel and buffer layer was observed with sub-micron-sized carbon inclusions in the kernel side, and isolated UCO particles were located in the buffer layer.
- APT data reveals segregation of Te and Ag at the UO-UC interface.
- The APT results confirm also selective association of specific elements for the two different U-phases. The UO phase showed presence of fission products such as Pd, Zr, Ce, Nd, Er, Dy, Gd, La, Y, Xe, and Sm, whereas the UC phase showed higher concentrations or segregation of Rh, Ru, Zr, Xe, Cd, In, Sn, Tc, and Nb. No Cs was detected during this investigation.

ACKNOWLEDGEMENTS

This work was sponsored by the U.S. Department of Energy, Office of Nuclear Energy, under U.S. Department of Energy Idaho Operations Office Contract DE-AC07-05ID14517, as part of the Advanced Reactor Technology Program and the National Users Facility Rapid Turnaround Program. The United States Government retains and the publisher, by accepting the article for publication, acknowledges that the United States Government retains a nonexclusive, paid-up, irrevocable, world-wide license to publish or reproduce the published form of this manuscript, or allow others to do so, for United States Government purposes.

The authors acknowledge Mr. James Madden and staff at Materials and Fuels Complex for FIB-TEM fabrication; Paul Demkowicz and Subhashish Meher for the review of this paper. Transmission electron microscopy work was carried out at the CAES Microscopy and Characterization Suite.

REFERENCES

[1] J. D. Hunn, Results from ORNL Characterization of Nominal 350 µm NUCO Kernels from the BWXT 69300 Composite, ORNL/CF-04/07.

[2] BWXT Nuclear Products Division, G73, Industrial Fuel Fabrication and Development Lot G73D-20-69302, March 2005.

[3] BWXT Nuclear Products Division, G73I, Industrial Fuel Fabrication and Development Lot G73I-14-69307, July 2008.

[4] W. Schenk and H. Nabielek, High-temperature reactor fuel fission product release and distribution at 1600 to 1800°C, Nucl Technol, v96, p.323, 1991.

[5] M. Barrachin, R. Dubourg, S. De Groot, M. P. Kissane, and K. Bakker, Fission-product behavior in irradiated TRISO-coated particles: Results of the HFR-EU1bis experiment and their interpretation, J Nucl Mater, v415, p.104, 2011.

[6] H. Kleykamp, Mikrosondenuntersuchungen zum Verhalten der Spalprodukte in hoch abgebrannten HTR-brennstoffen, Kernforschungszentrum Karlsruhe, Report KfK 2213.

[7] T. N. Tiegs, Fission Product Pd-SiC Interaction in Irradiated Coated Particle Fuels, ORNL/TM-7203.

[8] T. N. Tiegs, Fission product Pd-SiC interaction in irradiated coated-particle fuels," Nucl Technol, v57, p.389, 1982.

[9] K. Wright and I. J. van Rooyen, "EPMA of irradiated AGR1 TRISO fuel particles," Proceedings of HTR2016, Las Vegas, 2016.

[10] Demkowicz, P. A., J. D. Hunn, R. N. Morris, I. Van Rooyen, T. Gerczak, J. M. Harp, and S. A. Ploger, AGR-1 Post Irradiation, Examination Final Report, INL/EXT-15-36407, 2015.

[11] J. A. Aguiar and I.J van Rooyen, Studying Unirradiated TRISO-coated Particles from the Second Advanced Gas Reactor Experiment, Presentation at TMS 2017, San Diego, 2/26-3/2, 2017.

[12] S. Utsunomiya and R. Ewing, The fate of the epsilon phase (Mo-Ru-Pd-Tc-Rh) in the UO2 of the Oklo natural fission reactors, Radiochimica Acta, v94, p.749, 2006.

[13] Paul A. Demkowicz, Edward L. Reber, Dawn M. Scates, Les Scott, and Blaise P. Collin, First high temperature safety tests of AGR-1 TRISO fuel with the Fuel Accident Condition Simulator (FACS) furnace, J Nucl Mater, v464, p.320, 2015.